Magnetostrictive friction of graphene sheets embedded carbon film

Lei Yang [a], Kai Qi [a], Dongfeng Diao [b, *], Pengfei Wang [b], Peidong Xue [a]

[a] Key Laboratory of Education Ministry for Modern Design and Rotor-Bearing System, Xi'an Jiaotong University, Xi'an, 710049, China
[b] Institute of Nanosurface Science and Engineering (INSE), Shenzhen University, Shenzhen, 518060, China

ARTICLE INFO

ABSTRACT

We report a magnetostrictive friction phenomenon in atomic force microscopy (AFM) silicon probe sliding against graphene sheets embedded carbon (GSEC) film under external magnetic field. A special electromagnet device was designed on AFM to generate controllable magnetic field for the magnetostrictive friction measurements. GSEC films possessing self-magnetism were prepared by electron irradiation in electron cyclotron resonance (ECR) plasma. The magnetostrictive friction was investigated by adjusting the external magnetic field intensity and self-magnetism of the film. The results showed that the presence of the magnetic field resulted in an evident increment of the friction force of GSEC films with different magnetism, while the friction of nonmagnetic silicon wafer was not affected, indicating that the interaction between external magnetic field and the self-magnetism of the carbon film contributes to the friction increment, i.e. magnetostrictive friction. The mechanism of the magnetostrictive friction was ascribed to the atomic scale real contact area increment induced by the magnetostrictive strain of the graphene sheets. This finding may shed light on the new applications of magnetostrictive friction of carbon film.

© 2020 Elsevier Ltd. All rights reserved.

1. Introduction

Although micro-/nano-electromechanical systems (MEMS/NEMS) are known for decades, the tribological issues are yet the main challenge for the durable operation of MEMS/NEMS having parts in relative motion [1,2]. Therefore, control of friction and wear is essential for the development of contact MEMS/NEMS [3,4]. Nowadays, with the rapid development of electromagnetic techniques, an increasing number of MEMS/NEMS devices are working under an electromagnetic field [5–7], which brings new challenges for the tribological performance of these devices. The role of external magnetic field on the tribological properties of magnetic materials has been explored by numerous researchers [8–10]. According to previous studies, the magnetic field can influence friction in a variety of ways, including the generation of oxide film on the worn surface [11], lubrication of the wear debris [12], and magnetostriction effect [13]. However, present studies on the tribological properties under magnetic field are mainly conducted at the macroscale. There have been very few experimental investigations on the effect of magnetic field on the nanoscale friction. At nanoscale, the magnetic field-induced weak physical effects could have substantial effect on the mechanical and frictional behavior of the contact solids [14,15], which should be carefully considered while designing MEMS/NEMS. On the other hand, understanding such effect is beneficial to develop new methods to control nanoscale friction, which is a great deal of interest for improving the durability of MEMS/NEMS.

Owing to their excellent tribological characteristics, carbon-based materials have been increasingly regarded as ideal solid lubricants in MEMS/NEMS [16–18]. Especially since the discovery of graphene, it has received significant research attention in tribology due to its outstanding mechanical strength and friction reducing capabilities [19–21]. The frictional behavior of graphene is found to be affected by many factors, such as layer number [22,23], surface chemistry [24], sliding direction and speed [25,26], temperature [27], external strain [28,29], electric field [30]. Nevertheless, how to predictably control the friction of graphene remains a challenge in taking advantage of its promising properties. In the past few years, numerous works have proved the magnetism of graphene induced by unique electronic structures localized at topological defects or at special edges [31,32]. Besides, experimental and theoretical works predicted the magnetostriction effect of graphene in the presence of external magnetic field [33–35]. These findings provide a new possible approach to control the nano-friction of graphene-based

materials by magnetic field. Recently, our group found room-temperature magnetism of graphene sheets embedded carbon (GSEC) films prepared by electron irradiation assisted physical vapor deposition in electron cyclotron resonance plasma (ECR), which is induced by the spin magnetic moment at the edge of graphene sheets [36,37]. Moreover, this type of film also exhibited good tribological properties, making it a potential solid lubricant in MEMS/NEMS [38,39]. Therefore, it is of interest to investigate the nano-frictional behavior of GSEC film under external magnetic field.

Herein, an electromagnet was specially designed to perform atomic force microscopy (AFM) friction test under a controllable magnetic field. GSEC films were prepared with different electron irradiation energy in the ECR system to modulate the self-magnetism of the films. The nano-friction force of the AFM silicon probe sliding against GSEC film was measured under magnetic field. An evident friction increment of the GSEC films under the magnetic field was observed, i.e. magnetostrictive friction. The influence of external magnetic field intensity and self-magnetism of the film on the magnetostrictive friction was investigated. Further analysis was conducted to discuss the mechanism of the magnetostrictive friction effect.

2. Experimental details

2.1. Preparation of the GSEC film

The film was fabricated by using the low energy electron irradiation technique of an ECR plasma sputtering system. Detailed descriptions of the ECR system and the electron irradiation principle have been reported in our previous works [40], which are illustrated in Fig. S1. The film was deposited on silicon wafer with size of 20 mm × 20 mm × 0.5 mm, which was cleaned in acetone and ethanol bath successively by ultrasonic waves. The silicon wafer was fixed on a substrate holder inside the vacuum chamber of the ECR system. The pressure of the vacuum chamber was pumped down to 5×10^{-4} Pa and argon gas was inflated to keep a working pressure of 4×10^{-2} Pa. Then a stable plasma was generated by applying the 200 W microwave and magnetic field. The silicon substrate was bombarded by the argon ions to clean the surface by applying a negative substrate bias voltage of −50 V. After that, a bias voltage of −300 V was applied on the carbon target to generate carbon atoms for the film growth. During the deposition process, by tuning the substrate bias voltage, low electron irradiation with energy of 50, 100, and 150 eV was introduced to fabricate GSEC films. The deposition time was 25 min and the thickness of all the films was about 100 nm.

2.2. Characterization of materials

The nanostructures of the GSEC films were observed by using a transmission electron microscopy (TEM, JEM-2100) with 200 kV acceleration voltage. The TEM samples were prepared by scratching the GSEC film by a diamond pencil and transferring the flakes onto a copper micro grid. The bonding structures of the carbon films were characterized by Raman spectroscopy (HORIBA, HR-Resolution) using a 532 nm laser with spot size of 2 μm for excitation. The magnetic properties of the films were measured by a superconductivity quantum interference device (SQUID, MPMS-XL-7) at a constant temperature of 300 K. The magnetic field intensity was controlled between ±1 T. The surface morphologies of the samples were measured with atomic force microscopy (AFM, Dimension Edge, Bruker). The mechanical properties of the samples were tested by a nanoindenter (Hysitron TI-950) with a Berkovich diamond indenter with tip radius of 200 nm. The maximum

indentation load for all the tests was 150 μN. The hardness was then calculated by Oliver−Pharr method and the value was given by averaging three different measurement results.

2.3. Magnetostrictive friction measurements

Magnetostrictive friction measurements were performed with AFM (Dimension Edge, Bruker) using a CONTV-A silicon probe with tip radius of 8 nm. In order to apply external magnetic field during the measurements, an electromagnet was specially designed and installed on the sample stage of AFM, as shown in Fig. 1a. The size of the electromagnet was 135 mm × 130 mm × 30 mm, which fits the dimension of the AFM sample stage. The magnetic core and a pair of magnetic heads were made of electrical pure iron (DT-4). Copper wires were adopted to make the magnetic coils. The electromagnet was powered by a constant current source which could provide stable current from 0 A, to apply a continuously adjustable magnetic field on the sample starting from 0 mT. Fig. 1b illustrates the schematics of the magnetostrictive friction measurements on GSEC films. The sample was placed right between the two heads of the electromagnet on a 3D-printed sample holder (Material: acrylic monomer), guaranteeing the friction measurements could be operated under the magnetic field. The magnetic field was parallel to the sample surface. During the measurements, the friction force of an AFM silicon tip sliding against GSEC film with self-magnetism was measured in the presence of external magnetic field.

In order to characterize the magnetic field feature generated by the designed electromagnet, Ansoft Maxwell package was used to simulate the magnetic field distribution around the electromagnet. Fig. 1c shows the normalized magnetic field distribution. It is clear that the magnetic field is concentrated in the space between the two heads of the electromagnet and the magnetic field intensity between the two heads is nearly uniform, indicating that a strong and uniform magnetic field is present at the place where the sample is located during the friction test. A gaussmeter was used to measure the magnetic field intensity around the electromagnet with different coil current. Fig. 1d plots the magnetic field intensity as a function of the applying coil current measured at Position I, II, and III (as shown in the inset figures). Position I is located at the center between the two heads, Position II is in rear of Position I with a distance of 1 cm and inside the electromagnet structure, Position III is on top of Position I with a distance of 1 cm and higher than the top surface of the electromagnet. The results show that the magnetic field intensity increases almost linearly with the increase of the current at the three positions. Moreover, the intensity at Position I is much stronger than those at Position II and III, which matches quite well with the simulation results. In our friction tests, the AFM scanner is located on top of the electromagnet. Since the magnetic field intensity on top of the electromagnet is negligibly weak and the AFM silicon probe is nonmagnetic, the AFM can be normally operated without the influence of the applied magnetic field.

Before the friction measurements, force calibrations of the silicon tip were conducted. The normal force was calibrated by the thermal noise method [41]. The lateral force was calibrated on a Mikromasch TGF11 silicon grating by the improved wedge calibration method [42]. Details about the lateral force calibration are described in the Supporting Information (illustrated in Fig. S2). The friction loop was obtained by a complete trace and retrace scan over the same line with a length of 5 μm on the sample surface at a scanning speed of 1 μm/s. The scanning direction of the tip was perpendicular to the long axis of the cantilever. The friction force was then determined by calculating the half difference between the trace and retrace friction signals. Five repeated friction loop measurements along the same line were conducted under the same test
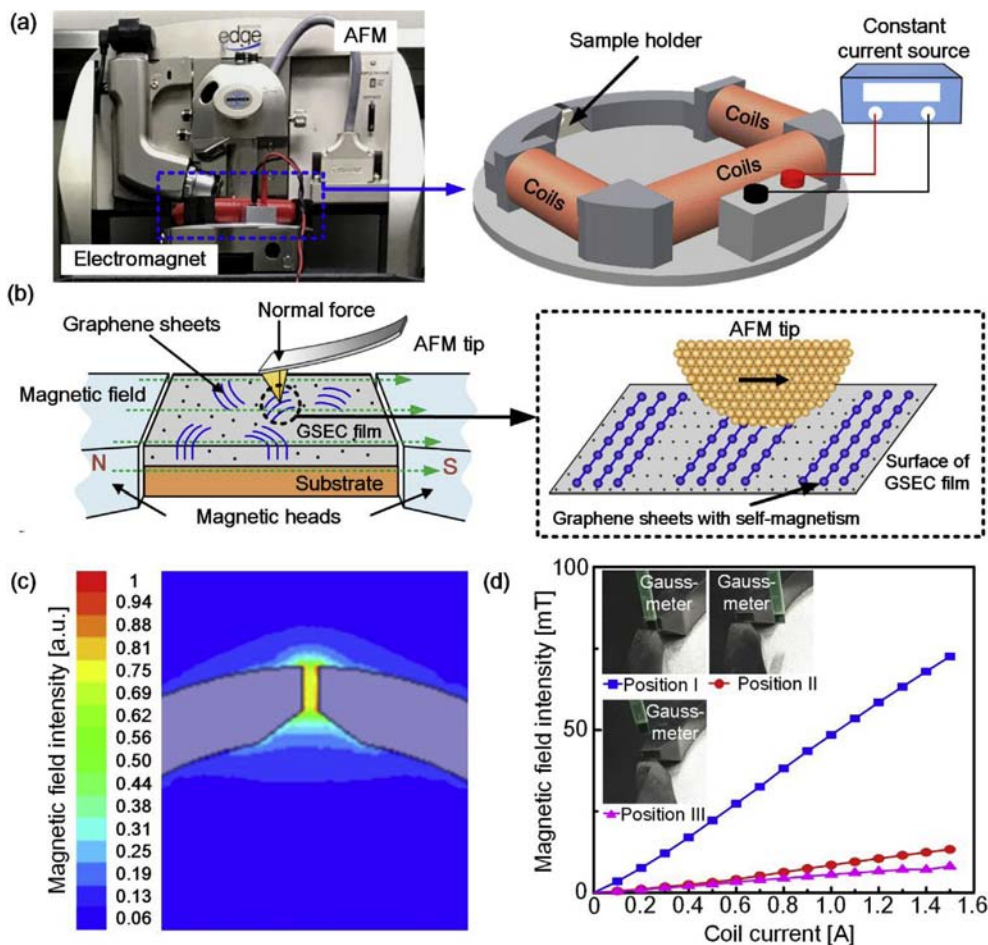
Fig. 1. Experimental setup for the magnetostrictive friction measurements. (a) AFM equipped with a specially designed electromagnet. (b) Schematics of the magnetostrictive friction measurements on GSEC films. (c) Normalized magnetic field distribution around the electromagnet simulated by the Ansoft Maxwell package. (d) Magnetic field intensity as a function of the coil current measured at three positions with gaussmeter. The inset figures are photographs of the three measurement positions. (A colour version of this figure can be viewed online.)

condition to determine the quantitative friction force. All of the friction tests were carried out at room temperature (25 °C) with relative humidity of 40%.

3. Results and discussion

3.1. Characterization of the GSEC film

Fig. 2a shows the Raman spectra and TEM image the GSEC film deposited under electron irradiation energy of 100 eV. The 2D band near 2700 cm^{-1}, separate D and G bands near 1340 cm^{-1} and 1600 cm^{-1} can be clearly observed in the Raman spectrum of the 100 eV irradiation film. The 50 eV and 150 eV irradiation samples have the similar Raman spectrum (as shown in Fig. S3). Such Raman spectral feature of the carbon film has been proved to be induced by the existence of graphene sheets. In the inset TEM image of the film, graphene nanocrystallites can be clearly observed, containing several graphene sheets. According to our previous works, the size of the graphene nanocrystallites in GSEC film becomes larger when the electron irradiation energy increases, which can be confirmed by the ratio of D peak intensity to G peak intensity (I_D/I_G) in the Raman spectrum [36,37]. To prove this, the D band and G band were fitted with a Lorentzian line and a Breit-Fano-Wagner (BFW) line [43], respectively. The value of I_D/I_G was then calculated according to the decomposed D and G band. It is found the values of I_D/I_G for

50, 100, and 150 eV irradiation samples are 0.84, 1.04, and 1.50, respectively, revealing that graphene nanocrystallite size increases with the irradiation energy. The magnetic properties of the films were measured by a SQUID MPMS-XL-7 at the constant temperature of 300 K. The magnetization curves ($M-H$ curves) of samples are depicted in Fig. 2b and a smaller field region of the curves are shown in the inset figure. Clear hysteresis loops can be observed for the three samples, revealing the magnetism of these graphene sheets embedded carbon films. Such self-magnetism of the film has been proved to originate from the excess electrons captured by the edge quantum well of the graphene sheets according to our previous works [44]. Moreover, saturation magnetizations M_s of the film becomes larger as the electron irradiation energy increases, indicating carbon films fabricated with higher electron irradiation energy exhibit stronger magnetism.

3.2. Friction of non-magnetic silicon under external magnetic field

Since an external electromagnet is equipped on AFM, in order to further confirm that the normal functions of AFM such as surface morphology scanning and friction force measurement are not affected by the magnetic field generated by the electromagnet, a non-magnetic silicon wafer was scanned by AFM under the external magnetic field. Friction loops were measured with the same probe scanning on the surface of the silicon wafer with a
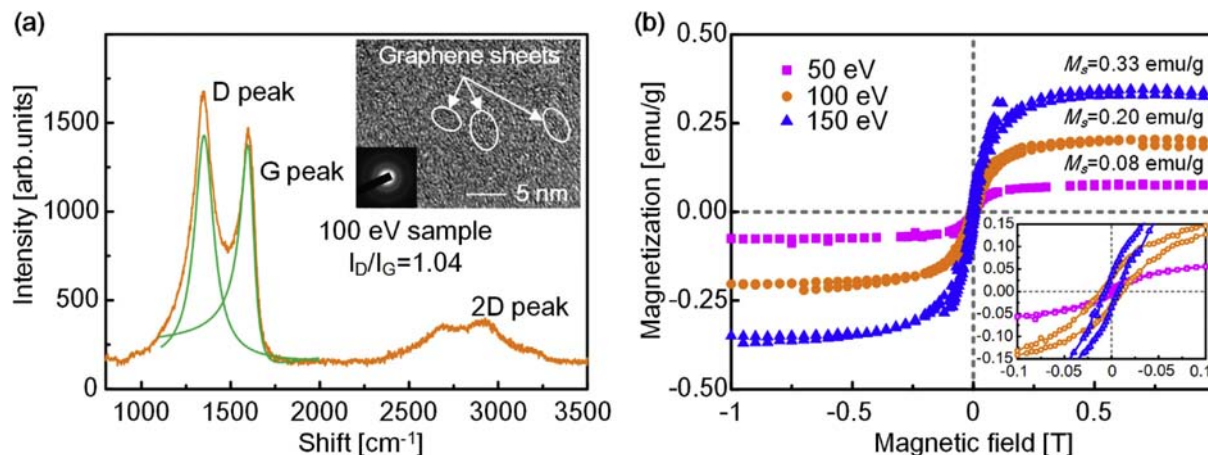
Fig. 2. Nanostructure and magnetism of GSEC film. (a) Raman spectra of the 100 eV irradiation GSEC film marked with the ratio of D band intensity to G band intensity I_D/I_G. Orange curve: the initial Raman spectra; green curves: decomposed D and G bands. The inset figure is the plan-view TEM image of the film. (b) Magnetization curves of GSEC films deposited with different electron irradiation energy (50, 100, and 150 eV). The inset figure shows a smaller field region of the hysteresis loops. (A colour version of this figure can be viewed online.)

constant normal force of 19.46 nN under different magnetic field (intensity: 0, 7.6, 17.0, and 27.4 mT). Fig. 3a shows the friction loops of the Si wafer measured at 0 mT and 17.0 mT under constant normal force of 19.46 nN. The applied magnetic field does not bring noticeable change in the friction loop. Then the quantitative friction force was calculated by multiplying the lateral force calibration constant with the mean half difference between trace and retrace signals. Fig. 3b gives the measured nano-friction force of the silicon wafer in relation to the applied magnetic field intensity. We can clearly see that the nano-friction force of the silicon wafer only shows slight fluctuations with the increment of the magnetic field intensity, indicating that the friction force of a nonmagnetic silicon wafer is not affected by the magnetic field. In addition, the surface morphology of Si was also measured under the magnetic field (as

shown in Fig. S4), and it is found that the surface morphology is not affected by the magnetic field. The above results demonstrate the AFM can be normally run under the magnetic field generated by the electromagnet.

3.3. Magnetostrictive friction of GSEC film with self-magnetism

The nano-friction forces of the GSEC films with self-magnetism were then measured by the above described AFM equipped with a specially designed electromagnet. Fig. 4a presents the surface morphology images of the 100 eV irradiation GSEC film scanned by the AFM under magnetic field intensity of 0 and 17.0 mT. The measured mean surface roughness values of the sample at 0 mT and 17.0 mT are 3.15 nm and 3.11 nm, respectively, suggesting the external magnetic field does not affect the normal operation of AFM on the magnetic GSEC samples. Then by controlling the external magnetic field intensity, friction loops of the sample were measured by the silicon tip over a line with a length of 5 μm at a scanning speed of 1 μm/s. Fig. 4b shows the friction loops of the 100 eV irradiation GSEC film obtained at 0 mT and 17.0 mT under constant normal force of 19.46 nN. Comparing the two friction loops, it is obvious that the difference between the trace and retrace friction signals increases when external magnetic field with intensity of 17.0 mT is applied during the test, implying that the applied magnetic field increases the friction force of the magnetic GSEC film. To quantitatively evaluate the effect of magnetic field on the frictional behavior of the GSEC film, the friction force was calculated by averaging the values measured by repeating the friction test five times with the same magnetic field intensity. Fig. 4c gives the friction force of 100 eV irradiation GSEC film in relation to the applied magnetic field intensity under normal force of 19.46 nN. We can clearly find that the external magnetic field strengthens the nano-friction of the magnetic GSEC film. And the friction force increases with the increment of the applied magnetic field intensity. At 0 mT, the friction force of the sample is 10.62 nN, and it increases to 14.49 nN at 27.4 mT, increased by 36.42%. Such phenomenon is named as magnetostrictive friction in this study. Compared with the measurement results on the nonmagnetic silicon wafer, it is obvious that the friction increment under magnetic field only occurs on magnetic GSEC film, indicating the magnetostrictive friction could be resulted from the interaction between external magnetic field and self-magnetism of the film. In addition,
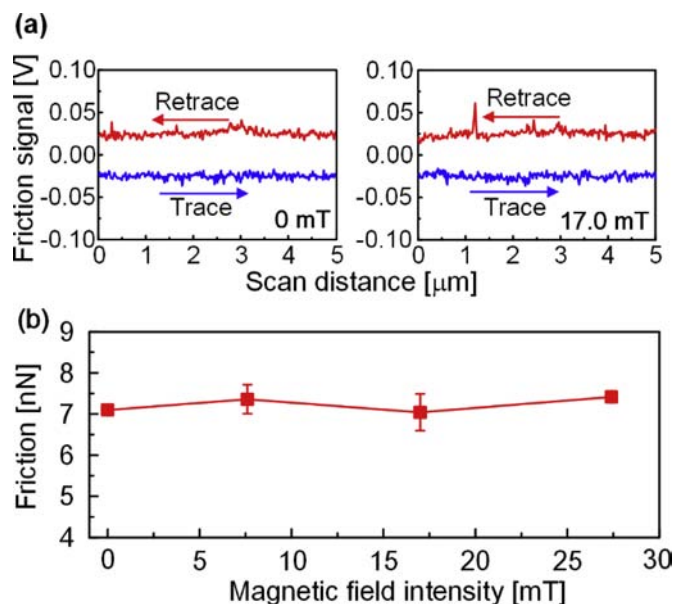
Fig. 3. Friction of the Si wafer under external magnetic field. (a) Friction loops of the Si wafer measured with magnetic field intensity of 0 mT and 17.0 mT under normal force of 19.46 nN. (b) Nano-friction force of the Si wafer as a function of the external magnetic field intensity with a constant normal force of 19.46 nN. (A colour version of this figure can be viewed online.)
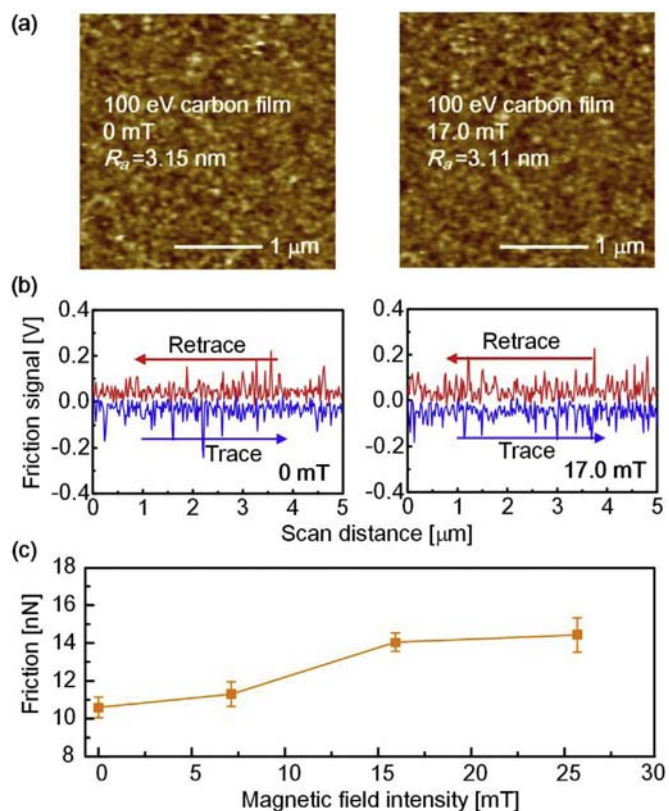
Fig. 4. Magnetostrictive friction of the 100 eV irradiation GSEC film. (a) Surface morphology of the 100 eV irradiation GSEC film measured by AFM with magnetic field intensity of 0 mT and 17.0 mT. (b) Friction loops of the 100 eV irradiation GSEC film measured with magnetic field intensity of 0 mT and 17.0 mT under normal force of 19.46 nN. (c) Nano-friction force of the 100 eV irradiation GSEC film as a function of the external magnetic field intensity under normal force of 19.46 nN. (A colour version of this figure can be viewed online.)

such magnetostrictive friction phenomenon of the GSEC film is also meaningful to the study on the tribological behavior of other carbon coatings. For instance, there are sp^2 bonds in diamond-like carbon (DLC) coatings [45]. These sp^2 bonds may exhibit similar magnetostrictive friction effect when the DLC coatings are exposed to external magnetic field.

As mentioned in Section 3.1, the self-magnetism of the GSEC film can be controlled by the electron irradiation energy during the film deposition process. Therefore, in order to explore the influence of the GSEC film magnetic property on the magnetostrictive friction, nano-friction forces of the GSEC films fabricated under different irradiation energy (50, 100, and 150 eV) were measured under the external magnetic field. Fig. 5a presents the measured friction force as a function of the applied magnetic field intensity under normal force of 19.46 nN for different GSEC film samples. All of the friction forces are the average values of five repeated friction tests under the same magnetic field intensity. We can see that all of the three curves show increasing tendency with the magnetic field intensity, indicating that the magnetostrictive friction effect also occurs for the 50 eV and 150 eV irradiation GSEC films. To quantitatively compare the magnetostrictive friction of these three types of GSEC films, the friction force increasing amplitudes of the samples under the strongest magnetic field (27.4 mT) were calculated, as shown in Fig. 5b. It is found that the friction increasing amplitudes for the 50 eV, 100 eV, and 150 eV samples are 32.83%, 36.42% and 54.53%, respectively. Comparing with the saturation magnetization M_s of the film, it is suggested that the magnetostrictive

friction is enhanced when the self-magnetism of the GSEC film becomes stronger. In Fig. 5a, it is also worth noting that GSEC films deposited with higher electron irradiation energy exhibit larger friction force. This could be attributed to the fact that GSEC film deposited under higher irradiation energy possesses softer and rougher surface. The measured hardness and surface roughness of these films are shown in Fig. S5.

To further validate the above-found magnetostrictive friction of the GSEC films, the friction force of the 100 eV sample was measured under different normal force with the applied magnetic field. Fig. 6 compares the measurement results of the 100 eV irradiation film under normal force of 19.46, 32.44, and 45.42 nN with controlled magnetic field (0, 7.6, 17.0, and 27.4 mT). As shown in Fig. 6a, with the same magnetic field intensity of 17.0 mT, the trace-retrace difference of the friction loop becomes larger as the applied normal force increases, indicating the friction force of the GSEC film sample goes up with the increment of the normal force under the external magnetic field. The quantitative friction forces under different conditions were then calculated and summarized in Fig. 6b. For normal forces of 19.46 nN and 32.44 nN, a clear ascending trend of the friction force can be found when the external magnetic field intensity increases. However, when the normal force increases to 45.42 nN, the nano-friction force of the 100 eV irradiation sample shows only slight fluctuation with the increase of the external magnetic field. Such unexpected fluctuation of the friction force can be explained as follows. As the normal force increases to a certain extent, it plays the leading role in determining the nano-friction force acting on the contact interface. As a result, the influence of magnetic field on the nano-friction, i.e. magnetostrictive friction will be weakened. This can also be proved by the measurement results under normal force of 19.46 nN and 32.44 nN. At the strongest external magnetic field (27.4 mT), the increasing amplitudes of the friction force under normal force of 19.46 nN and 32.44 nN are 36.42% and 12.75%, respectively. It is apparent that larger normal force weakens the magnetostrictive friction of the GSEC films under magnetic field.

Based on the present nano-friction test results, it is evident that the nano-friction of GSEC film is strengthened under the external magnetic field. In order to interpret the mechanism of such phenomenon, a schematic illustration is drawn to explain the effect of the magnetic field on the nano-frictional behavior of the GSEC film, which is related to the magnetostriction effect of the graphene sheets under external magnetic field, as shown in Fig. 7. According to Mo et al.'s work [46], the friction force at nanoscale depends linearly on the number of atoms that chemically interact across the contact, which is used to define the real contact area at the nanoscale. Therefore, strain engineering provides a means of controlling nanoscale friction, since the real contact area of the nano contact pair could be tuned by applying an external strain on the solid. The external strain effect on the nano-frictional behavior of graphene has already been proved in Li et al.'s work [28] and our previous molecular dynamics simulations [29]. Here, in our experiments, when there is no magnetic field applied during the nano-friction test, the real contact area between the AFM tip and the GSEC film is defined to be $A_{real} = N_{at}A_{at}$, where N_{at} is the number of atoms of the sample within the range of chemical interactions from the tip atoms (the atoms in the red circle as shown in Fig. 7a) and A_{at} is the average surface area per atom. When the magnetic field is applied, the atoms of the film within the contact zone are compressed due to the magnetostrictive strain of the graphene sheets under the interaction between external magnetic field and the self-magnetism of the carbon film, as illustrated in Fig. 7b. In consequence, the number of 'contacting' atoms N_{at} increases. In other words, the real contact area increases, thus leading to the increment of the nano-friction force of GSEC film, which is named as
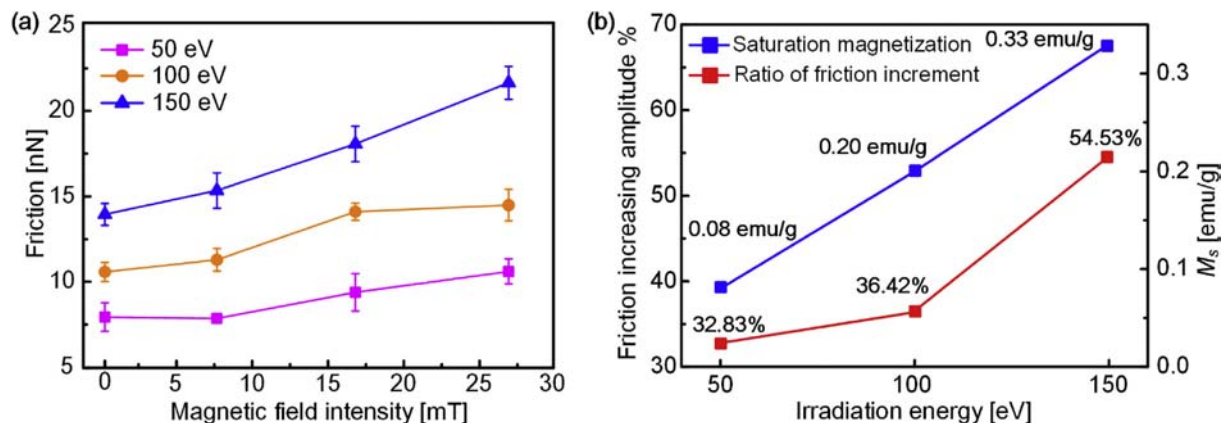
Fig. 5. Magnetostrictive friction of GSEC films with different magnetism. (a) Nano-friction force of different GSEC films (50, 100, and 150 eV) as a function of the external magnetic field intensity under normal force of 19.46 nN. (b) Quantitative comparison of the magnetostrictive friction of different GSEC films. (A colour version of this figure can be viewed online.)
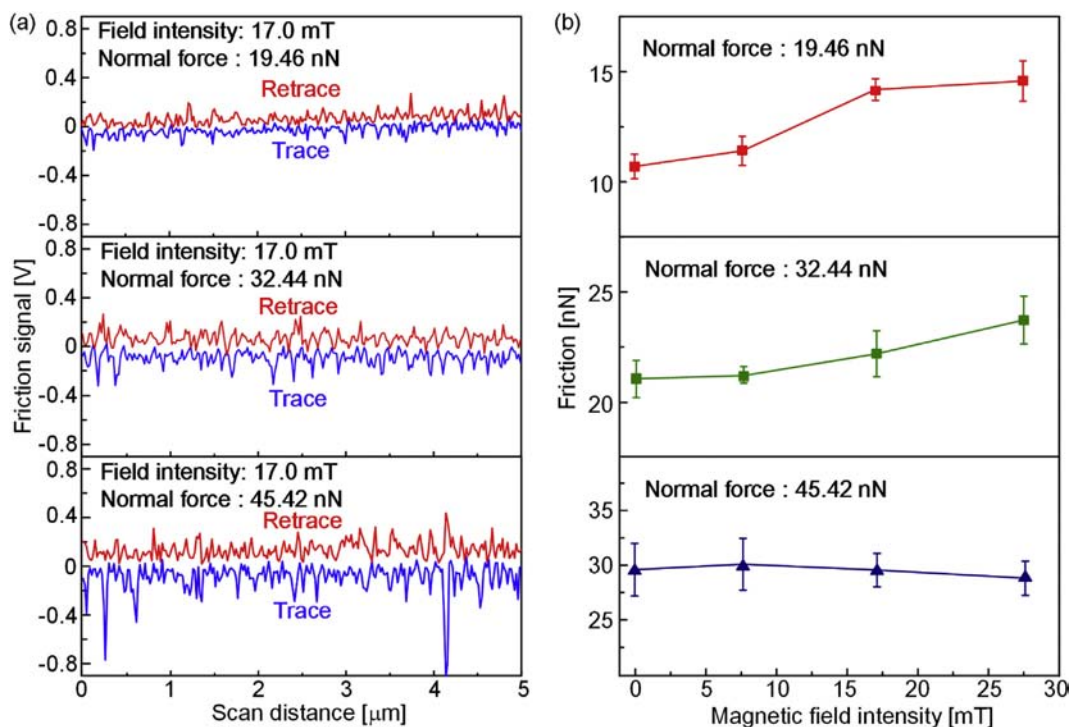
Fig. 6. Dependence of magnetostrictive friction on normal force. (a) Friction loops of the 100 eV irradiation GSEC film measured with magnetic field intensity of 17.0 mT under normal force of 19.46, 32.44, and 45.42 nN. (b) Nano-friction force of the 100 eV irradiation GSEC film as a function of the external magnetic field intensity under different normal force. (A colour version of this figure can be viewed online.)

magnetostrictive friction in this paper. This also explains the larger friction increment for the film with stronger magnetism. When the self-magnetism of the GSEC film increases, the magnetostrictive strain of graphene sheets become larger under the same external magnetic field, leading to more increment of the real contact area. Therefore, the magnetostrictive friction is enhanced as the self-magnetism of the GSEC film increases.

In order to validate the mechanism that the magnetostrictive strain of the graphene sheets is responsible for the friction increment under the magnetic field, external compressive strain was introduced into the GSEC film and then friction forces of these pre-strained films were measured by AFM. The GSEC film with thickness of 100 nm was transferred on flexible polydimethylsiloxane (PDMS) substrate, which was then fixed on a 3D-printed concave

mold (Material: acrylic monomer) to apply compressive strain to the transferred GSEC film. The strain is determined by changing the curvature radius (r) of the concave mold ($\varepsilon \propto 1/r$) [47]. Details about the sample preparation process are shown in Fig. S6. Friction measurements were carried out in the central area of each transferred sample with scan distance of 2 μm to avoid the potential influence of the curvature effect of the concave mold [48]. Fig. 8 gives the friction force of the transferred GSEC film (100 eV irradiation) in relation to the curvature ($1/r$) of the mold under normal force of 19.46 nN. Obviously, the friction force of the film goes up as the curvature of the mold (i.e., compressive strain) increases, indicating that the external compressive strain results in friction increment of the GSEC film. In addition, the friction force of the transferred 100 eV irradiation GSEC is larger than that of the film on
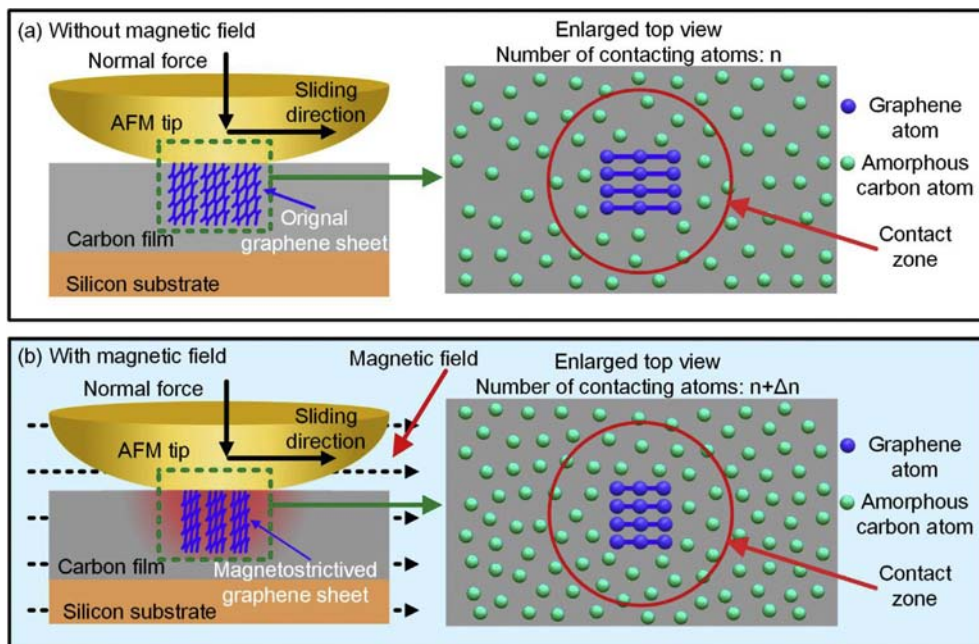
Fig. 7. Schematics of the mechanism of the magnetostrictive friction. (a) State of the contact between the GSEC film and the AFM silicon tip without magnetic field. The right figure shows the atom arrangement at the contact interface. (b) State of the contact between the GSEC film and the AFM silicon tip with magnetic field. The right figure shows the magnetostriction effect-induced variation of the real contact area. (A colour version of this figure can be viewed online.)
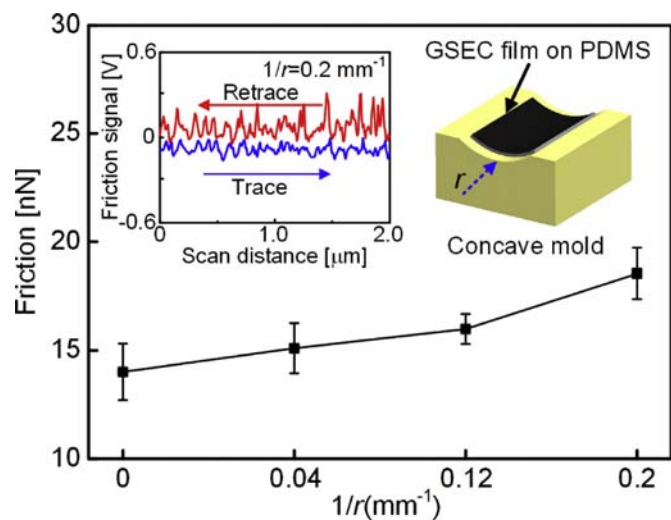
Fig. 8. Nano-friction force of the transferred 100 eV irradiation GSEC film as a function of the curvature ($1/r$) of the concave mold under normal force of 19.46 nN. The inset figures give the friction loop of the film on a mold with curvature of 0.2 mm^{-1} and schematics of the transferred film on the concave mold. (A colour version of this figure can be viewed online.)

a Si substrate, which is probably because the PDMS substrate is softer than Si. The above results provide evidence to support our mechanism on the magnetostrictive friction.

4. Conclusions

In summary, a new method to measure magnetostrictive friction under external magnetic field is developed utilizing atomic force microscopy (AFM) equipped with a specially designed electromagnet. Graphene sheets embedded carbon (GSEC) films were fabricated by low energy electron irradiation technique of an ECR

plasma sputtering system and were proved to possess magnetism at room temperature by SQUID measurements. Through the magnetostrictive friction measurements on GSEC films with different magnetism under different magnetic field intensity, an evident increment of the friction force of GSEC films under external magnetic field was found, named as magnetostrictive friction. Such phenomenon was related to interaction between external magnetic field and self-magnetism of the films. It was found that larger magnetic field intensity and stronger self-magnetism could both enhance the magnetostrictive friction of GSEC films. For the film with the strongest magnetism in the present work (150 eV irradiation film), the friction force under normal force of 19.46 nN was increased by 54.53% with the maximum magnetic field intensity (27.4 mT). Further analysis was conducted to discuss the mechanism of the magnetostrictive friction. It was inferred that the atomic real contact area increment at the contact interface caused by the magnetostrictive strain of the graphene sheets under the magnetic field was responsible for the friction increment. These findings enrich the understanding of friction mechanism and open up a new door for the friction control of carbon film.

CRediT author statement

Lei Yang: Conceptualization, Investigation, Validation, Data Curation, Writing - Original Draft, Kai Qi: Investigation, Validation, Writing - Original Draft, Dongfeng Diao: Supervision, Writing - Review & Editing, Pengfei Wang: Validation. Peidong Xue: Validation.

Declaration of competing interest

The authors declare that they have no known competing financial interests or personal relationships that could have appeared to influence the work reported in this paper.

Acknowledgements

Appendix A. Supplementary data

Supplementary data to this article can be found online at https://doi.org/10.1016/j.carbon.2020.01.005.

References

[1] S.H. Kim, D.B. Asay, M.T. Dugger, Nanotribology and MEMS, Nano Today 2 (2007) 22—29.
[2] M. Urbakh, E. Meyer, Nanotribology: the renaissance of friction, Nat. Mater. 9 (2010) 8—10.
[3] B. Bhushan, Nanotribology and nanomechanics, Wear 259 (2005) 1507—1531.
[4] O. Hod, E. Meyer, Q.S. Zheng, M. Urbakh, Structural superlubricity and ultra-low friction across the length scales, Nature 563 (2018) 485—492.
[5] M. Glickman, P. Tseng, J. Harrison, T. Niblock, I.B. Goldberg, J.W. Judy, High-performance lateral-actuating magnetic MEMS switch, J. Microelectromech. Syst. 20 (2011) 842—851.
[6] M. Ganzhorn, S. Klyatskaya, M. Ruben, W. Wernsdorfer, Strong spin—phonon coupling between a single-molecule magnet and a carbon nanotube nano-electromechanical system, Nat. Nanotechnol. 8 (2013) 165—169.
[7] K. Kim, J.H. Guo, X.B. Xu, D.L. Fan, Micromotors with step-motor characteristics by controlled magnetic interactions among assembled components, ACS Nano 9 (2015) 548—554.
[8] J.L. Jiang, Y. Tian, Y.G. Meng, Role of external magnetic field during friction of ferromagnetic materials, Wear 271 (2011) 2991—2997.
[9] H.B. Han, S.M. Du, Y.Z. Zhang, H. Liu, R.M.R. Pan, Effect of DC magnetic field on friction and wear properties of 45 steel at different velocities, Tribol. Lett. 64 (2016) 38.
[10] J.Y. Xu, J.L. Mo, X.C. Wang, X. Zhang, D.W. Wang, Z.R. Zhou, Effects of a horizontal magnetic field on unstable vibration and noise of a friction interface with different magnetic properties, Tribol. Int. 120 (2018) 47—57.
[11] L.C. Fu, L.P. Zhou, Effect of applied magnetic field on wear behaviour of martensitic steel, J. Mater. Res. Technol. 8 (2019) 2880—2886.
[12] H. Zaidi, M. Amirat, J. Frene, T. Mathia, D. Paulmier, Magnetotribology of ferromagnetic/ferromagnetic sliding couple, Wear 263 (2007) 1518—1526.
[13] A. Babutskyi, A. Chrysanthou, C.L. Zhao, Effect of pulsed magnetic field pre-treatment of AISI 52100 steel on the coefficient of sliding friction and wear in pin-on-disk tests, Friction 2 (2014) 310—316.
[14] H. Zhou, H.L. Zhang, Y.M. Pei, H.S. Chen, H.W. Zhao, D.N. Fang, Scaling relationship among indentation properties of electromagnetic materials at micro- and nanoscale, Appl. Phys. Lett. 106 (2015), 081904.
[15] J. Zhang, L.L. An, B. Zhang, J.Y. Zhang, Y.L. Yu, C.M. Wang, Interlayer friction properties of oxygen-doped hexagonal boron nitride bilayers, Europhys. Lett. 127 (2019) 16003.
[16] W.Z. Zhai, N. Srikanth, L.B. Kong, K. Zhou, Carbon nanomaterials in tribology, Carbon 119 (2017) 150—171.
[17] P. Manimunda, A. Al-Azizi, S.H. Kim, R.R. Chromik, Shear-induced structural changes and origin of ultralow friction of hydrogenated diamond-like carbon (DLC) in dry environment, ACS Appl. Mater. Interfaces 9 (2017) 16704—16714.
[18] H. Xu, J. Al-Ghalith, T. Dumitrica, Smooth sliding and superlubricity in the nanofriction of collapsed carbon nanotubes, Carbon 134 (2018) 531—535.
[19] D. Berman, A. Erdemir, A.V. Sumant, Graphene: a new emerging lubricant, Mater. Today 17 (2014) 31—42.
[20] N. Chan, S.G. Balakrishna, A. Klemenz, M. Moseler, P. Egberts, R. Bennewitz, Contrast in nanoscale friction between rotational domains of graphene on Pt(111), Carbon 113 (2017) 132—138.
[21] M. Tripathi, F. Awaja, R.A. Bizao, S. Signetti, E. Iacob, G. Paolicelli, et al., Friction and adhesion of different structural defects of graphene, ACS Appl. Mater. Interfaces 10 (2018) 44614—44623.
[22] C. Lee, Q.Y. Li, W. Kalb, X.Z. Liu, H. Berger, R.W. Carpick, et al., Frictional

[23] L. Yang, Q. Zhang, D.F. Diao, Cross-linking-induced frictional behavior of multilayer graphene: origin of friction, Tribol. Lett. 62 (2016) 33.
[24] T. Arif, G. Colas, T. Filleter, Effect of humidity and water intercalation on the tribological behavior of graphene and graphene oxide, ACS Appl. Mater. Interfaces 10 (2018) 22537—22544.
[25] J.S. Choi, J.S. Kim, I.S. Byun, D.H. Lee, M.J. Lee, B.H. Park, et al., Friction anisotropy—driven domain imaging on exfoliated monolayer graphene, Science 333 (2011) 607—610.
[26] X.Z. Zeng, Y.T. Peng, L. Liu, H.J. Lang, X.A. Cao, Dependence of the friction strengthening of graphene on velocity, Nanoscale 10 (2018) 1855—1864.
[27] R.C. Sinclair, J.L. Suter, P.V. Coveney, Graphene-graphene interactions: friction, superlubricity, and exfoliation, Adv. Mater. 30 (2018) 1705791.
[28] S.Z. Li, Q.Y. Li, R.W. Carpick, P. Gumbsch, X.Z. Liu, X.D. Ding, et al., The evolving quality of frictional contact with graphene, Nature 539 (2016) 541—545.
[29] L. Yang, Y.J. Guo, Q. Zhang, Frictional behavior of strained multilayer graphene: tuning the atomic scale contact area, Diam. Relat. Mater. 73 (2017) 273—277.
[30] H.J. Lang, Y.T. Peng, G.W. Shao, K. Zou, G.M. Tao, Dual control of the nano-friction of graphene, J. Mater. Chem. C 7 (2019) 6041—6051.
[31] R.R. Nair, I.L. Tsai, M. Sepioni, O. Lehtinen, J. Keinonen, A.V. Krasheninnikov, et al., Dual origin of defect magnetism in graphene and its reversible switching by molecular doping, Nat. Commun. 4 (2013) 2010.
[32] H. Gonzalez-Herrero, J.M. Gomez-Rodriguez, P. Mallet, M. Moaied, J.J. Palacios, C. Salgado, et al., Atomic-scale control of graphene magnetism by using hydrogen atoms, Science 352 (2016) 437—441.
[33] H. Wang, A.C. Papageorgopoulos, N. Garcia, Defects in graphite may be magnetic and magnetostrictive as revealed by scanning tunneling microscopy, Eur. Phys. J. B 40 (2004) 499—504.
[34] H. Santos, A. Ayuela, L. Chico, E. Artacho, van der Waals interaction in magnetic bilayer graphene nanoribbons, Phys. Rev. B 85 (2012) 245430.
[35] J. Zhu, H. Park, R. Podila, A. Wadehra, P. Ayala, L. Oliveira, et al., Magnetic properties of sulfur-doped graphene, J. Magn. Magn. Mater. 401 (2016) 70—76.
[36] C. Wang, D.F. Diao, Self-magnetism induced large magnetoresistance at room temperature region in graphene nanocrystallited carbon film, Carbon 112 (2017) 162—168.
[37] C. Wang, X. Zhang, D.F. Diao, Nanosized graphene crystallite induced strong magnetism in pure carbon films, Nanoscale 7 (2015) 4475—4481.
[38] C. Chen, D.F. Diao, X. Fan, L. Yang, C. Wang, Frictional behavior of carbon film embedded with controlling-sized graphene nanocrystallites, Tribol. Lett. 55 (2014) 429—435.
[39] C. Chen, P.D. Xue, X. Fan, C. Wang, D.F. Diao, Friction-induced rapid restructuring of graphene nanocrystallite cap layer at sliding surfaces: short run-in period, Carbon 130 (2018) 215—221.
[40] C. Wang, D.F. Diao, X. Fan, C. Chen, Graphene sheets embedded carbon film prepared by electron irradiation in electron cyclotron resonance plasma, Appl. Phys. Lett. 100 (2012) 231909.
[41] J.L. Hutter, J. Bechhoefer, Calibration of atomic-force microscope tips, Rev. Sci. Instrum. 64 (1993) 1868—1873.
[42] M. Varenberg, I. Etsion, G. Halperin, An improved wedge calibration method for lateral force in atomic force microscopy, Rev. Sci. Instrum. 74 (2003) 3362—3367.
[43] S.D.M. Brown, A. Jorio, P. Corio, M.S. Dresselhaus, G. Dresselhaus, R. Saito, et al., Origin of the Breit-Wigner-Fano lineshape of the tangential G-band feature of metallic carbon nanotubes, Phys. Rev. B 63 (2001) 155414.
[44] X. Zhang, C. Wang, C.Q. Sun, D.F. Diao, Magnetism induced by excess electrons trapped at diamagnetic edge-quantum well in multi-layer graphene, Appl. Phys. Lett. 105 (2014), 042402.
[45] X.D. Li, B. Bhushan, Micromechanical and tribological characterization of hard amorphous carbon coatings as thin as 5 nm for magnetic recording heads, Wear 220 (1998) 51—58.
[46] Y.F. Mo, K.T. Turner, I. Szlufarska, Friction laws at the nanoscale, Nature 457 (2009) 1116—1119.
[47] Y. Zhang, L.K. Shen, M. Liu, X. Li, X.L. Lu, L. Lu, C.R. Ma, C.Y. You, A.P. Chen, C.W. Huang, L. Chen, M. Alexe, C.L. Jia, Flexible quasi-two-dimensional CoFe2O4 epitaxial thin films for continuous strain tuning of magnetic properties, ACS Nano 11 (2017) 8002—8009.
[48] S. Zhang, Y. Hou, S.Z. Li, L.Q. Liu, Z. Zhang, X.Q. Feng, Q.Y. Li, Tuning friction to a superlubric state via in-plane straining, Proc. Natl. Acad. Sci. U.S.A. 116 (2019) 24452—24456.